Elastic Properties of Random-Linked *cis*-PB Networks: A Characterization and Gel Point Study

W. PYCKHOUT-HINTZEN,* B. MÜLLER, and T. SPRINGER

Forschungszentrum Jülich GmbH, Institut für Festkörperforschung, Postfach 19 13, 5170 Jülich, Germany

SYNOPSIS

cis-Polybutadiene networks with microstructure 98% *cis*, cross-linked in the bulk state by gamma irradiation, were characterized in terms of their mechanical properties. Data from stress–strain analyses, swelling degrees, stress relaxation, and random-linking theory are in accordance and the estimated gel points practically coincide. Trapped entanglements lead to a 30% increase in the network modulus, from which also the plateau modulus, 0.71 ± 0.09 MPa, was determined. The tensile data were obtained from Mooney–Rivlin representations without junction constrained corrections. Preliminary stress-relaxation experiments indicated a slow relaxation at room temperature. It can be concluded that the assumption of additive contributions from chemical and entanglement cross-link densities in the Langley theory works well in the range of doses investigated here. © 1993 John Wiley & Sons, Inc.

INTRODUCTION

Rubber elasticity of deformed networks is determined by the configuration of the strands between chemical junctions (cross-links) that covalently connect different chains. The interpenetration of chains, however, gives rise to possible "topological" or "physical" cross-links that contribute to the measured stress response. Therefore, in the interpretation of stress–strain experiments, a clear distinction has to be made between chemical and physical cross-links, which can be "transient" or "trapped," respectively. The cross-links are transient if their contribution to the equilibrium modulus disappears at low frequency or for long times; they are called "trapped" if they persist for an infinite time. The aim of this experimental study was the characterization of a randomly cross-linked network using different techniques, separating the cross-link contributions into their respective parts.

The elastomer under investigation is a polybutadiene (PB)-(98% *cis*)-network that was cross-linked by gamma irradiation. Several studies of PB networks, differing in *cis*-content as well as cross-linking procedure, have been published.[1-10] The importance of entanglements has been a matter of controversy. While Dossin and Graessley[4] discussed a highly entangled network structure with dominating topological contributions for atactic PB networks, cross-linked under gamma radiation, Hsu and Mark,[8] Su and Mark,[3] and Brotzman[7] came to the conclusion that the elastic modulus is hardly affected by local contacts and can be described by merely hindered cross-link motion. Our study extends over a gamma dose up to 21 Mrad and covers the cross-linking from the critical gel point up to an almost completely cross-linked material. The trapped "topology" will be compared to the melt plateau modulus of *cis*-PB, G_N^0, derived from stress–strain experiments, stress relaxation, and from sol–gel extraction of the network state.

Determination of Network Parameters

For a rubber material, the shear modulus is defined as $G(\lambda) = \sigma(\lambda)/(\lambda - \lambda^{-2})$, with $\lambda = L/L_0$, the ratio of sample lengths after (L) and before (L_0) tension. In the limit for small deformation, we obtain $G(\lambda \to 1) = G_c$, with

$$G_c = A(\rho/M_c)(1 - 2M_c/M_n)RT \qquad (1)$$

* To whom correspondence should be addressed.

Journal of Applied Polymer Science, Vol. 48, 887–896 (1993)
 CCC 0021-8995/93/050887-10

The index c means that chemical cross-links are involved only. M_c is the mean molecular weight of the strands between chemical cross-links, corrected for mechanically neutral free chain ends, and M_n, the number-average length of the chains before cross-linking. (ρ/M_c) is equal to (ν/V), the number of strands ν per unit volume V. ρ is the bulk density. A is the so-called front-factor. For freely fluctuating phantom networks with ϕ-functional junctions, A is found to be $(\phi - 2)/\phi$.[11] A is near unity for a severely hindered motion of the cross-links due to local restrictions. The Kuhn model corresponds to $A = 1$ or $\phi = \infty$. The quantity $\sigma(\lambda)$ is the nominal stress, i.e., the stress related to the initial unstretched cross section.

Pervasions of chains in a melt will inevitably lead to nonpermanent entanglements that can be viewed as tetrafunctional junctions. In the rubbery plateau, therefore, the elastic reversibility is as complete as in a chemically cross-linked network.[12] The modulus, here, is

$$G_e = (\rho/M_e)RT \tag{2}$$

where M_e is the average molecular weight between such entanglements in the uncross-linked melt. The total retractive force of a real network is determined by the combination of both chemical cross-link and topological entanglement densities, which contribute to the rubbery modulus. In the Langley approach,[13] additivity of these contributions, i.e., of the inverse strand lengths, is assumed and the resulting shear modulus is

$$G = G_c + G_t = G_c + G_e t_e \tag{3}$$

t_e, the trapping factor, distinguishes between the total number of entanglements (leading to G_e) and the actually frozen-in entanglements (G_t). Estimates for t_e can be obtained from a statistical description of the gelation process as proposed by Dossin and others[2,4,14,15] in terms of the fraction of monomers taking part in cross-links (q) and those taking part in scission reactions (p) during irradiation cross-linking:

$$t_e = [1 - (2/N_n q) - 2(p/q)]^2 \tag{4}$$

The sol fraction, w_s, of a network, is a complicated function of p, q; the polydispersity index $\beta = (N_w/N_n) - 1$; and the kinetic length of the cross-linking–polymerization reaction upon radiation, $(1/i)$. N_n and N_w are the number and weight averages of the degrees of polymerization, respectively. Following Refs. 2 and 4, w_s is given by

$$w_s = \frac{1}{\left(a + \frac{p}{q}\right)^3}\left\{\frac{2a\left(\frac{p}{q}\right)}{qN_w}\left(\frac{1+\beta}{\beta}\right) + \left(a + \frac{p}{q}\right)\left(\frac{p}{q}\right)^2 - \frac{2a\left(\frac{p}{q}\right)}{qN_w}\left(\frac{1+\beta}{\beta}\right)\left(1 + qN_w\frac{\left(a + \frac{p}{q}\right)}{1+\beta}\right)^{-\beta} + a^2\left(a + \frac{p}{q}\right)\left(1 + qN_w\frac{\left(a + \frac{p}{q}\right)}{1+\beta}\right)^{-(1+\beta)}\right\} \tag{5}$$

and $a = 1 - w_s i^3[1 - (1 - i)w_s]^{-3}$. The number of chemical cross-links per chain is then obtained from qN_n. This implies that the tensile properties will be dominated by the shorter molecules. M_c is then $[M_n/(qN_n + 1)]$.

The evaluation of the total modulus in stress–strain experiments can be adequately modeled by the semiempirical Mooney–Rivlin approximation as[16,17]

$$\sigma(\lambda)/(\lambda - \lambda^{-2}) = 2C_1 + 2C_2/\lambda \tag{6}$$

with $2C_1$ and $2C_2$ as two empirical constants. The reduced stress, $\sigma(\lambda)/(\lambda - \lambda^{-2})$, is often written as σ^*. In the limit of small deformations ($\lambda \simeq 1$), the initial modulus $G_0 = 2C_1 + 2C_2$ also includes contributions from transient topological entanglements. For the extrapolation to large deformations ($\lambda \gg 1$), G, according to eq. (3), reduces to $2C_1$.

The same information is obtained independently from stress-relaxation data over sufficient long observation times at different temperatures, for which the relaxation modulus is approximated by

$$G(t) = G_\infty + \sum_i G_i e^{-(t/\tau_i)} \tag{7}$$

which means that, according to this equation, $G_\infty = 2C_1$. The relaxation times τ_i are usually attributed to dangling end motion and cross-link reorganization.[11,17]

Similar results, though less conclusive, may be drawn from isotropic swelling of the dry network in a good solvent.[18] Here, the stretching of the chains leads to the calculation of cross-link densities from

$$(\rho/M_c) = \frac{(-\ln(1 - v_{2m}) - v_{2m} - \chi_1 v_m^2)}{(1 - 2/\phi)V_1 v_{2s}^{2/3} v_{2m}^{1/3}} \tag{8}$$

in the phantom network model. v_{2m} and v_{2s} are the volume fractions of network and solvent, respec-

tively.[3,6] V_1 and χ_1 stand for the molar volume of the solvent molecules and their interaction parameter with the polymer. Its use is limited, however, by the lack of reliable values of χ_1.

In our experimental evaluation of the structure of the PB network, the use of eq. (3) will be central: The separation of chemical and physical contributions depends on the trapping factor, t_e, which itself is obtained after fitting the gel curve to a cross-linking rate as a function of the irradiation dose using eq. (5). The agreement of G_c or, equivalently M_c, in all analyses then proves the consistency and the assumption of the Langley approach [eq. (3)].

EXPERIMENTAL

GPC Characterization

The molecular weight distribution of the commercial *cis*-PB (Aldrich), with a *cis*-content 98.6%, was measured by gel permeation chromatography (Waters GPC) in THF at 35°C, equipped with three columns of porosities in the range 10^5, 10^4, and 10^3 Å and consisting of three units: a 600E pump system, a 490E UV, detector and a 410E Waters differential refractometer. The carrier solvent was THF and the elution rate, constant over time, was 1 mL/min. A calibration curve was determined from selected Polybutadiene Standards (Polysciences) between 500 and 300,000 g/mol. M_n and M_w were 97,000 and 242,000 g/mol; the peak molecular weight was at 169,000 g/mol. GPC distributions were investigated as a function of dose. Weight distributions shown in Figure 1 correspond to doses between 0 and 2 Mrad. The gel point at which the molecular weight of the gel becomes infinite is situated between 1.5 and 1.8 Mrad (*vide infra*). Here, the contribution to the high molecular weight side is increased considerably. The 1.8 and 2.0 Mrad curves show the expected behavior beyond the gel point: The gel is insoluble. It was removed from the distribution by carefully filtering the solutions that cause a narrowing of the wing at high molecular weights. The wing broadening on the low molecular weight side is indicative of scission reactions upon radiation. The estimated uncertainty in the M_w scale is about 10% (Table I). The distributions were normalized for the sake of comparisons only.

Intrinsic Viscosity

The intrinsic viscosity, $[\eta]$, was determined in cyclohexane from five dilute solutions well below the estimated c^* ($c^* \cong 0.004$ g cm^{-3}). $[\eta]$ was linearly extrapolated from (η_{sp}/c) to $(c = 0)$. The cyclohexane was freshly distilled from sodium/antracene/BuLi. The Mark–Houwink relationship used was

$$[\eta] = 3.87\ 10^{-2} M^{0.697} \quad \text{at } T = 25°C$$

and yielded $[\eta] = (178 \pm 5)$ mL/g or $\bar{M}_w = (179{,}870 \pm 9000)$ g/mol. After correction for the polymolec-

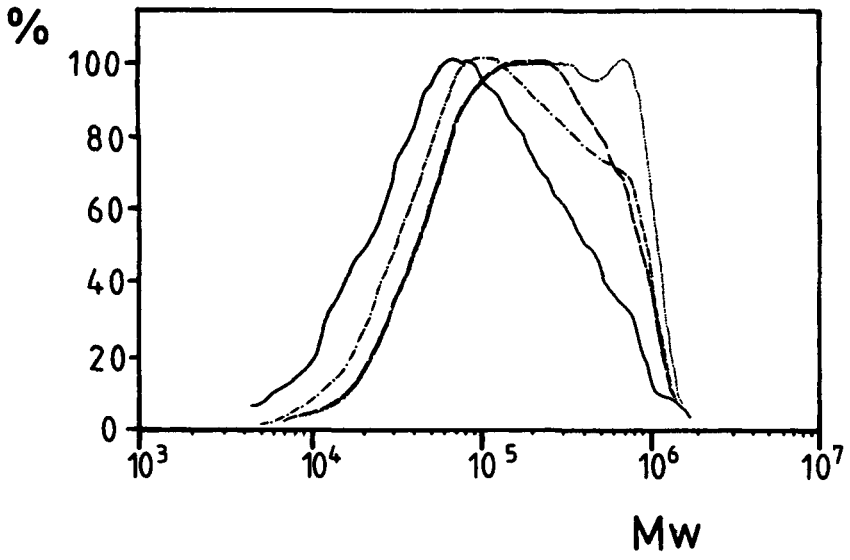

Figure 1 GPC trace, normalized to 100% output signal in dn/dc units to correct for concentration effects. Lines correspond to different radiation doses: (– – –) 0 Mrad; (· · · ·) 1.5 Mrad; (– · – · –) 1.8 Mrad; (——) 2.0 Mrad. The gel dose is situated between 1.5 and 1.8 Mrad as indicated by the clear broadening and narrowing at high M_w, respectively.

Table I Sample Characterization before Cross-linking

Method	M_n (g/mol)	M_w (g/mol)	$\frac{M_w}{M_n}$	$[\eta]$ (mL/g)
GPC	97,000	242,000	2.5	—
Intrinsic viscosity	82,000[a]	205,000	—	178 ± 5

[a] Dependent parameter, determined from M_w/M_n (GPC).

ularity, estimated from the GPC measurements with $M_w/M_n = 2.5$, assuming a Schultz–Zimm–Flory distribution, we obtained $M_w = (205{,}000 \pm 11{,}000)$ g/mol, in reasonable agreement with the data from the gel-permeation chromatography (GPC).

Network Formation by γ-Radiation

cis-PB, as purchased from Aldrich Co., was dissolved in dry toluene without further fractionation. The concentrated solution with a polymer volume fraction $v_{2m} \simeq 0.5$ was kept for a few days until most of the solvent had evaporated. The remaining polymer fraction was about 0.85. Thin films of approximately 2 mm were obtained after subsequent drying under vacuum at room temperature. In this way, the formation of air bubbles was avoided. The resulting polymer fraction was 0.96 or higher. Different batches were prepared for irradiation near fuel elements from the research reactor FRJ-2 in the KFA Jülich. The γ-activity was about 2.92×10^{15} photons per second, with their main energy contribution around 0.7 MeV. The samples were sealed in watertight containers and stored under water in the radiation field, at dose rates of 0.09 and 0.15 ± 0.1 Mrad/h. The dose was measured by Schott glass dosimeters, calibrated by the known radiation (about 3000 Curie) of a Cs-137 source. The samples were yellow after the highest applied doses. Dumbbell-shaped samples were then cut of the irradiated material; their length-to-width ratio was close to 6.

Sol–Gel Determination and Swelling in Benzene

From each sample, two strips of different size were swollen in dry benzene at $T = 23 \pm 1$°C. After 3 days, equilibrium was obtained and the weight of the swollen species was determined by quickly transferring it to a balance. The external solvent was wiped off. The samples were then dried under vacuum at $T = 55 \pm 3$°C for 3 days, and their individual weight was remeasured. The gel fraction was then obtained from the difference between initial and final weight. The same samples were then reswollen in THF for another 2 days to ensure that all sol fraction had been extracted. After drying under vacuum, only small differences (less than 2%) were found for the lowest-dose samples. The yellow color also disappeared in the solvents, indicating that it was (partly) due to unattached low molecular weight material. The gel fraction w_g is given in Figure 2. Additivity of volumes in the swollen state was assumed. The gel point is clearly identified in Figure 2 by the disappearance of w_g at a dose of 2 Mrad, which is consistent with the qualitative results of GPC in Figure 1.

Elastic Deformation in Instron Machine

Stress–strain experiments were performed on a dynamic Instron 1342 machine. It is controlled by hydraulics with two Servo-cylinders that move symmetrically about a central point. A load cell is mounted on the lower moving cylinder. Its inertia is measured by an attached accelerometer and the load signal is internally corrected. Nitrogen, gas or liquid, is passed through a thermostat and directed onto the sample. The sampling rate was adjusted to gather 6000 data points during the strain phase. Strain rate ($d\epsilon/dt$) and maximum extension are input into the program interactively. Strain ϵ and $\lambda = (L/L_0)$ were determined in separate experiments from spots 1 and 2 cm away from the center of the sample. Reference samples served as a further check of the sensitivity and absolute calibration of the load cell. Force fluctuations were 0.3–0.6 N. Relaxation experiments were performed well above the glass temperature after a steady and rather rapid deformation of typically 10 s. No significantly different results were obtained if the ramp time was 3–5 s and data were monitored after 0.1–0.5 s.

Stress–strain data were obtained during a continuous strain period with constant strain rate $d\epsilon/dt$. Figure 3 presents the reduced stress $\sigma^* = \sigma(\lambda)/(\lambda - \lambda^{-2})$ in a typical Mooney–Rivlin representation vs. $(1/\lambda)$ from which the empirical constants may be easily computed for the different doses between 4.5 and 21 Mrad. No upturn due to crystallization

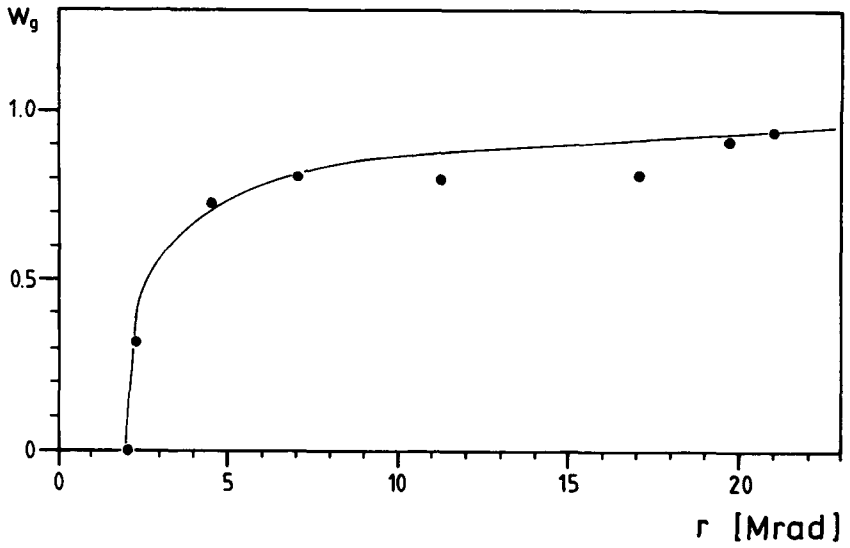

Figure 2 Gel fraction w_g vs. dose, obtained after extraction with benzene and THF. The gel dose is estimated as 1.95 Mrad. The solid line corresponds to a fitted model with eq. (7) and describes the complete dose range continuously.

of segments could be found at the maximum elongation ($\lambda = 3$) and T even about $-10°C$. The crosshead speed v was selected to be 0.016 mm/s or, correspondingly, strain rates about 10^{-3}/s were found appropriate. The crosshead speed was optimized to minimalize the $2C_2$ parameter in the Mooney plots and investigated between 0.05 and 100 mm/s. Figure 4 shows the result. The influence of rapid stretching levels off below a critical velocity v_c of the order 0.05–0.15 mm/s[19] and depends on the radiation dosage. The intercept of σ^* or $2C_1$ did not depend on $d\epsilon/dt$ as expected since dynamic contributions are factored out as in eq. (6).

RESULTS

Sol–Gel Analysis

In the evaluation of the sol–gel curve data, we assumed a linear relationship between linking/scission

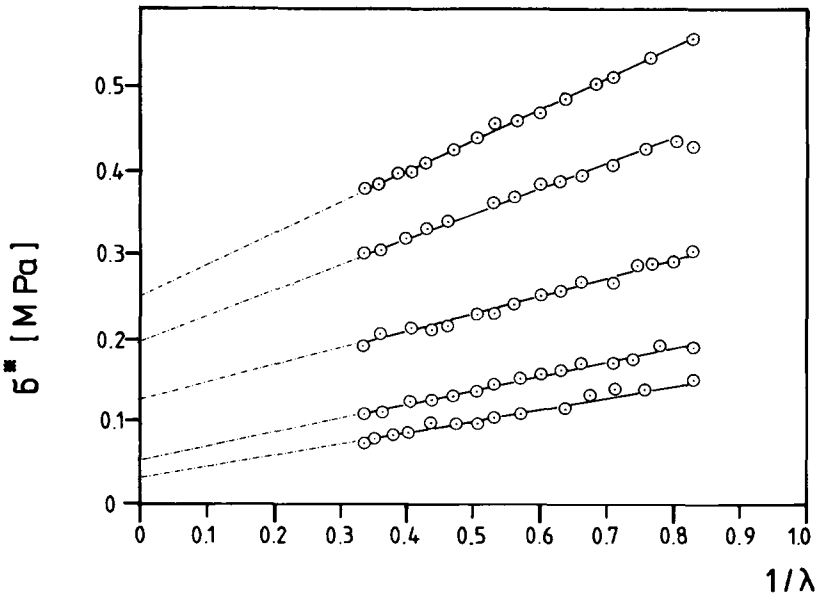

Figure 3 Mooney–Rivlin plot, i.e., reduced stresses σ^* vs. $1/\lambda$. Data correspond in decreasing intercept to doses 21, 17, 11.2, 7, and 4.5 Mrad, respectively.

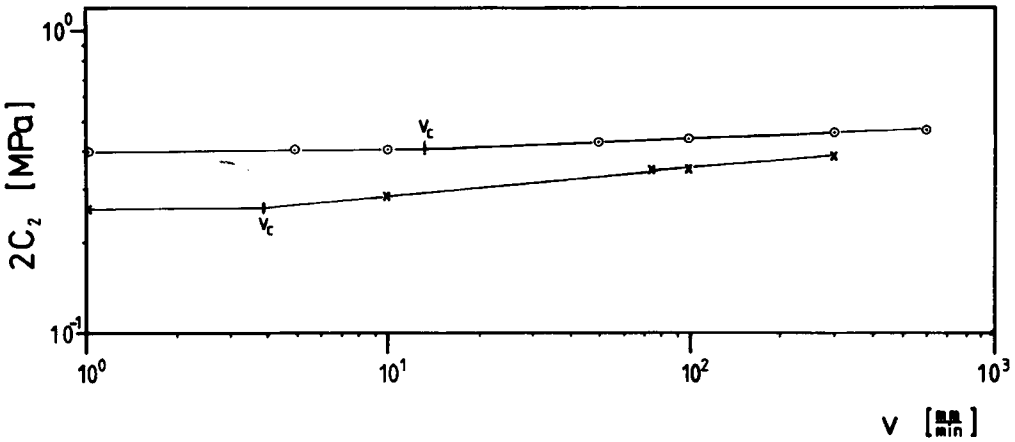

Figure 4 The Mooney–Rivlin parameter $2C_2$ vs. crosshead speed v for samples with dose (⊙) 21 Mrad and (x) 19.7 Mrad. Critical crosshead speeds v_c were estimated from the intersection of two linear regimes at lower and higher v. Below v_c no strain rate dependency is expected anymore.

and the radiation dose, namely, $q = q_0 r$ and $p = p_0 r$, which were substituted in eq. (5) for w_s. The quantitities q_0 and (p_0/q_0) were fitted iteratively at fixed $1/i$ until consistency was reached. The polymerization degrees as derived from the GPC distribution were used. The experimental data and the best-fit gel curve is presented in Figure 2 as a function of the radiation dose r. The error is of the order of 5%. At high doses, the very low extractable content is apparent as well as the gel point near $r_{gel} \cong 2.0$ Mrad. The best-fit values for q_0 and (p_0/q_0) are (1.14 ± 0.09) and $(0.033 \pm 0.010) \times 10^{-4}$ Mrad^{-1}, respectively, yielding $p_0 = (3.76 \pm 1.12) \times 10^{-6}$ Mrad^{-1}, which cover the complete dose range. Interestingly, the kinetic chain length $1/i$, which represents the number of monomers added to the radical before termination, could be varied from 1.00 to 1.12 with no significant changes in the best-fit values for q_0 and (p_0/q_0). This assures that the average functionality of the function is situated between 4.0 and 4.5. Reported higher functionalities[7,20] are not observed or do not influence this conclusion significantly.

For our computations, perfect tetrafunctional cross-linking was assumed. With $q = q_0 r$ and $\mu = qN_n$, the number of chemical cross-links per chain of length N_n may be calculated, and for the free-fluctuating phantom case, transformation in M_c is made. The network parameters so obtained and the corresponding trapping factor [eq. (9)] are summarized in Table II.

In the high-dose limit ($q = \infty$, $r = \infty$), eq. (5) approaches $w_s = 0$. The critical gel dose r_{gel} may be thought of as the dose at which an infinitively long molecule is formed. However, there still coexists a lot of smaller clusters of molecules. The dose is obtained by extrapolation of the gel curve to $w_g = 0$ (or $w_s = 1$), which yields $r_{gel} = (1.8 \pm 0.2)$ Mrad

Table II Theoretical Chemical Network Parameters from Sol–Gel Statistics; Ideality of the Network Was Assumed

Dose (Mrad)	w_g Exp	w_g Theo	$q \cdot 10^3$	$\mu = q \cdot N_n$	ν	t_e	M_c (g/mol)
21	0.95	0.955	2.390	4.43	8.86	0.12	9,217
19.7	0.92	0.949	2.250	4.16	8.32	0.09	9,690
17.0	0.82	0.930	1.940	3.59	7.18	0.05	10,893
11.2	0.80	0.880	1.280	2.36	4.72	0.01	14,881
7.0	0.81	0.810	0.798	1.48	2.96	—	20,161
4.5	0.73	0.705	0.513	0.95	1.90	—	25,641
2.3	0.32	0.375	0.262	0.48	0.97[a]	—	(103,093)

[a] Approximates end-linking.

with $q = 2.05 \times 10^{-4}$. This is in excellent agreement with the Flory gelation density for random linking, estimated as $q \simeq 1/N_w$, which yields 2.22×10^{-4} or $r_{gel} = 1.95$ Mrad. Our former estimate from the GPC trace yielded ($1.5 \leq r_{gel} \leq 1.8$) Mrad or ($1.7 \times 10^{-4} \leq q \leq 2.1 \times 10^{-4}$), respectively.

Mooney–Rivlin Analysis

The reduced stress σ^* as defined earlier [eq. (6)] at $T = 23°C$ for our samples is presented in Figure 3 as a function of $1/\lambda$. Only a few representative data points are shown. The maximal elongation was fixed at $\lambda = 3$ to prevent crystallization.[21] The final polymer volume fraction, v_{2m}, after removing the solvent, was set to 1.00 in view of the last weighing ($v_{2m} = 0.96$) prior to cross-linking. The corresponding correction term ($v_{2m}^{2/3}$) in the stress, therefore, does not show up in eq. (1). The strain rate was optimized as described and the results can be considered as equilibrium data. The curves exhibit a perfect linear behavior up to high deformations, which justifies the semiempirical treatment of the reduced stress following eq. (6).[16,22] No evidence for the junction-constraint model of Flory and Erman[23–25] could be found, which would lead to a more or less pronounced sigmoid-shaped dependency of σ^* with $1/\lambda$. Neither varying the polymer volume fraction nor any acceptable parameter fit of the constraints itself, which led to physical unreasonable values, could confirm this theory.

Consequently, the intercept values $2C_1$ from the Mooney–Rivlin analysis were identified with the phantom shear modulus of the network following eq. (1). They are higher than expected from our results of the sol–gel curve. This means that topological cross-links do play a role and thus contribute to $2C_1$.

The modulus, G_c, corresponding to the chemical cross-links, therefore was calculated from $2C_1$, after diminishing by t_eG_e. For G_e, we adopted the plateau modulus G_N^0 for high *cis*-PB as determined by Ferry (0.76 MPa).[26] t_e was taken from the sol extraction data in Table II. After this correction, chemical strand lengths, M_c, now agree very well with the sol–gel data with a mean deviation below 12%, as shown in Tables II and III.

In addition, $2C_1$ vs. the radiation dose is presented in Figure 5. Two linear regimes are visible that could be approximated by one linear regression line: The analysis of all six data points up to small $2C_1$ values by one straight line with correlation 99.8% yields the gel point at $r_{gel} = (2.1 \pm 0.2)$ Mrad, in good agreement with our determinations by GPC and the random-linking theory, eq. (5). The presence of two slopes, however, implies further diversification. Tentatively, we therefore separate $2C_1$ at low dosages as G_c ($r \leq 7$ Mrad), where entanglement trapping is only effective by less than 1% according to the calculations.

Under this assumption, the gel point is situated at $r_{gel} = 1.74 \pm 0.20$ Mrad, closer to the values quoted before. The slope of $2C_1$ vs. dose r, which is $2 N_n q_0 RT/V$ (since $\nu = 2\mu$),[27] is in excellent agreement with the estimate for q_0 obtained from fitting eq. (5).

The slope of the dose dependence of $2C_1$ for $r \geq 7$ Mrad, however, increases significantly. This is supposed to be due to topological entwining of segments on different chains. Its contribution can be estimated from the difference between the (higher) experimental values of $2C_1$ and the fitted line for low doses, $G_c = -0.0174 + 0.010r$ [Mrad], at the gamma dosage in question.

The topological terms G_t are then 0.058, 0.046, and 0.005 MPa for the 21, 17, and 11.2 Mrad samples, respectively. The mean topological modulus G_e is computed from (G_t/t_e) and yields $G_e = 0.64 \pm 0.25$ MPa. This means that from the numerical values of G_t and Figure 5 it is clearly recognized that the

Table III Mooney–Rivlin Analysis

Dose (Mrad)	$2C_1$ (MPa)	$2C_2$ (MPa)	M_c (g/mol) (a)	M_c (g/mol) (b)
21.0	0.251 ± 0.007	0.301 ± 0.014	5,574	8,233
17.0	0.199 ± 0.010	0.309 ± 0.011	7,206	8,661
11.2	0.125 ± 0.002	0.208 ± 0.009	12,612	14,095
7.0	0.053 ± 0.003	0.172 ± 0.004	45,743(*)	45,743(*)
4.5	0.027 ± 0.002	0.146 ± 0.007	46,600(*)	46,600(*)

Strand-lengths, M_c, were computed from $2C_1$. (a) M_c, corrected for pendant chains only. (b) M_c, as (a) but corrected for entanglement contribution following eq. (3). (*) no correction used, since doubtful chemistry/sample.

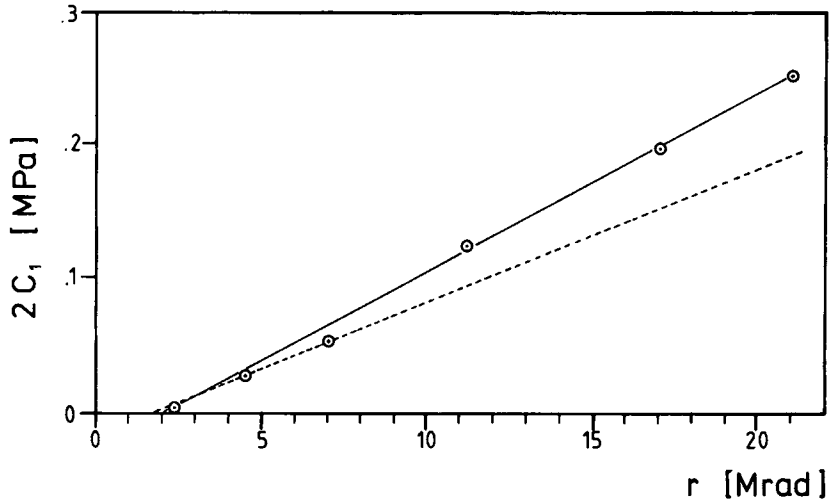

Figure 5 The Mooney–Rivlin parameter $2C_1$ vs. dose. The solid line (——) is a linear approximation over the whole range r [Mrad], extrapolating to the gel point dose at 2.1 Mrad. (- - -) A gel point determination, corrected for entanglements appearing at doses $\geq$ 7 Mrad (i.e., $t_e > 0$), yields 1.75 Mrad.

influence of the physical network of entanglements on the total modulus G is not negligible and varies between a 5 and 30% contribution in our radiation dose range. From the definition of t_e in eq. (4), the probability of trapping increases with the radiation dose r as $1 - c/r$, c being a constant, which causes also the relative contribution t_eG_e to increase considerably in the dose range investigated. Only at higher doses does t_e approach unity and constant contribution. Also, data on the low-deformation limit may yield the same information. The Langley plot as suggested by eq. (3) is reformulated to give

$$(G_0/t_e) = X(G_{c,\mathrm{ph}}/t_e) + G_e \qquad (9)$$

The least-squares optimization yielded $X = 0.95 \pm 0.07$ and $G_e = 0.69 \pm 0.05$ MPa. The close agreement of G_e cannot be accidential and suggests that the topological interactions act like chemical cross-links, favoring a Langley-type analysis. Comparable results are obtained here, in both limits of the strain, and may indicate a more complex distribution of their contribution to $2C_1$ and $2C_2$.

The slope, $2C_2$, in Figure 3 is indicative for non-equilibrium processes arising from relaxing topological constraints and is not interpreted in the present context. The tendency of $2C_2$ to increase with dose and therefore with topological contributions t_eG_e is also found.[1]

Stress-Relaxation

Stress-relaxation experiments were carried out on networks obtained with a dose $r \geq 7$ Mrad. The strain was approximated as $(1/3)(\lambda - \lambda^{-2})$ instead of $(\lambda - 1)$.[26] Moduli for temperatures −10, 24, and 40°C were reduced to a common reference temperature $T_0 = 24$°C and rescaled by

$$G_{\mathrm{red}}(t) = G(t)(\rho_{T_0}T_0/\rho_T T) \qquad (10)$$

ρ_{T_0}/ρ_T was calculated from the molar volume expansion coefficients. The time axes of the curves were then scaled by the WLF factor a_T[28]:

$$a_T = A(T - T_0)/[B + (T - T_0)] \qquad (11)$$

with $A = 3.44$ and $B = 196.6$ as determined by Ferry for a high-*cis*-(96%)-PB.[26] No further adjustment was attempted. The relaxation curve extends between 10^{-2} and 10^4 s over six orders of magnitude and is shown for a typical sample (7 Mrad) in Figure 6. The "collapse" of the data on one curve is fairly good with the quoted scaling factor. The relaxation function is then decomposed as in eq. (7), from which the plateau moduli G_∞ were obtained by either extrapolation to long relaxation times or by means of a fitting procedure to eq. (7). This fitting clearly established, for all samples, the existence of at least two characteristic times: a short one that is situated around $\tau_1 \simeq 70 \pm 30$ s including entanglements of transient nature and a much slower relaxation with $\tau_\infty \simeq 800 \pm 200$ s. These time scales are well separated and may open the possibility to investigate the reorganization of cross-links far apart or changes in chain dimensions. Also, the distinction between local processes and dangling end relaxation could

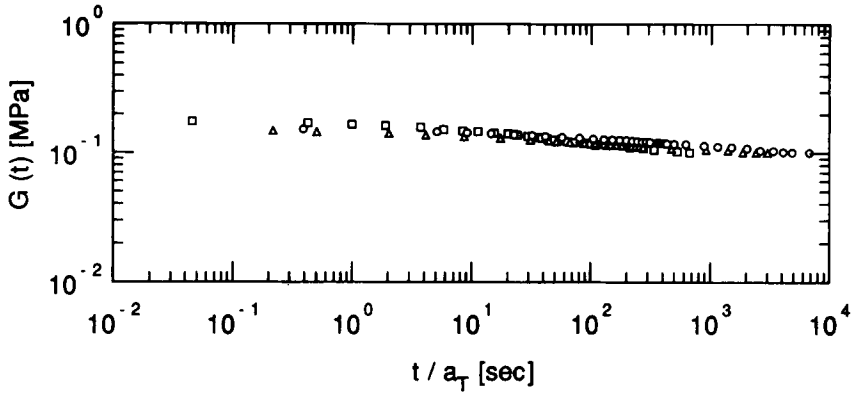

Figure 6 Time-dependent stress–relaxation moduli $G(t)$ vs. t, reduced to $T_0 = 24°C$ for the 7 Mrad sample: (□) $T = -10°C$; (△) $T = 24°C$; (○) $T = 40°C$.

become clear. Since the longer times, τ_α, do not differ significantly among all samples despite varying amounts of dangling end-defects, motion on a larger scale might be more realistic. Equilibrium plateau values, G_α, are given in Table IV with corresponding strand lengths corrected for frozen-in entanglements. The agreement with Mooney–Rivlin data ($2C_1$) and sol–gel curve data is good. Also, the 7 Mrad sample now agrees well with the chemical cross-linking density as calculated from the radiation chemistry. The average derivation from the theoretical treatment is about 16%. Tentatively, the ratio M_e to M_c with $M_e \cong 2900$ g/mol from rheology was plotted against G_α. At $M_e = M_c$, the plateau modulus G_N^0, for which the topological contribution should become indistinguishable from the chemical counterpart in the network, is 0.825 ± 0.05 MPa. This is in accord with compliance measurements by Ferry,[26] who deduced $G_N^0 = 0.758$ MPa and our estimates from the Langley plot (0.63 MPa). The atactic-PB melt exhibits a plateau modulus of 1.2 MPa with a correspondingly higher entanglement density. The use of the published value for G_N^0 (*cis*-PB) in the correction for the topological contributions throughout the analysis instead of our values is not critical.

Table IV Relaxation Equilibrium Plateau Moduli G_α

Dose (Mrad)	G_α (MPa)	M_c (g/mol) (a)	M_c (g/mol) (b)
21.0	0.294	7,238	9,275
17.0	0.286	7,499	8,199
11.2	0.177	11,092	11,408
7.0	0.100	16,741	16,741

The reference temperature is $T_0 = 24°C$. Estimated uncertainties are 10%. (a) No correction for topological contribution included. (b) Corrected following eq. (3).

Equilibrium Swelling Degrees

Volume fractions at swelling equilibrium at 25°C in benzene are given in Table V. The gel weight fraction was taken into account in the calculation of the swelling degree and the obtained chain densities in the phantom limit were transformed in strand lengths, M_c. Only corrections for the dangling end structure were undertaken. For this high-*cis*-PB, the values 0.21 (Ref. 6) and 0.265 (Ref. 7) for χ_1 have been proposed. Despite the fact that the latter is just the average of 0.21 and 0.32, the agreement with stress–strain data, relaxation, and sol–gel analysis is good. An extra contribution of entanglements does not appear to be necessary. Since the choice of χ_1 is fairly arbitrary, no special use of this additional information, which is used very often to characterize quickly the cross-link density, is made. The average deviation relative to the theoretical strand length is about 16%. It is to be noted that the agreement with the sol–gel determination is perfect if we substitute

Table V Swelling Data on Benzene at $T = 23°C$

Dose (Mrad)	ν_{2m}	M_c (g/mol) $\chi_1 = 0.21$	M_c (g/mol) $\chi_1 = 0.265$
21.0	0.104	6,424	8,025
17.0	0.099	7,186	8,930
11.2	0.078	12,212	15,764
7.0	0.052	35,102	53,254

Correction is made for pendant chains only. For parameter definition, see text.

an optimized $\chi_1 = 0.33 \pm 0.03$ as suggested already in earlier work by Su and Mark.[3]

CONCLUSION

We have presented a joint analysis of different techniques to characterize a random-linked *cis*-PB network after gamma-irradiation at different doses. The applied dose range has allowed complete investigation between gel point ($w_g = 0$) and an almost complete network ($w_g \cong 0.95$) in terms of mechanical properties, swelling degrees, and random-linking theory. A comparison of these methods was possible by a calculated "trapping factor" and the published plateau modulus for *cis*-PB.

The gel points obtained from an extrapolation of $2C_1$, the sol–gel curve, and GPC-distribution curves agree well within error limits and serve as an internal check. Following the Langley model where contributions from (permanent) chemical junctions and permanent trapped physical junctions are additive, the analysis revealed up to 30% increase of G due to entangled chains. The entanglement part of the modulus, G_e, was determined and yielded 0.71 ± 0.09 MPa on the average, compared to the plateau modulus 0.76 MPa from melt rheology. Preliminary stress-relaxation studies indicated a slow relaxation mode with $\tau \sim 700$ s, which is believed to result from cross-link reorganization.

The authors are grateful to G. Pohl and U. Bünten for their help with the Instron setup, to C. Pictroski (Exxon) for the redetermination of the *cis*-content, as well as J. Sissano (Exxon) for the assistance at his GPC facility. Also, R. Hoffmann (KFA Jülich) is thanked for irradiating the samples and W. Friedrich (KFA Jülich) for the calibration of the dosimeters.

REFERENCES

1. G. Kraus and G. A. Moczvgemba, *J. Pol. Sci. Part A*, **2,** 227 (1964).
2. D. S. Pearson, B. J. Skutnik, and G. A. Boehm, *J. Pol. Sci. Polym. Phys. Ed.*, **12,** 925 (1974).
3. T. K. Su and J. E. Mark, *Macromolecules,* **10,** 120 (1977).
4. L. M. Dossin and W. W. Graessley, *Macromolecules,* **12,** 123 (1979).
5. J. E. Mark and M. A. Llorente, *Polym. J.*, **13,** 543 (1981).
6. S. Saeki, J. C. Holste, and D. C. Bonner, *J. Pol. Sci. Polym. Phys. Ed.*, **20,** 794 (1982).
7. R. W. Brotzman and P. J. Flory, *Macromolecules,* **20,** 351 (1987).
8. Y. H. Hsu and J. E. Mark, *Polym. Prepr.*, **27,** 1 (1986).
9. R. Stadler, F. Buehler, and W. Gronski, *Makromol. Chem.*, **187,** 1301 (1986).
10. G. Friedmann and J. Brossas, *Eur. Polym. J.*, **20,** 1151 (1984).
11. H. M. James and E. Guth, *J. Chem. Phys.*, **15,** 669 (1947); **21,** 1039 (1953).
12. D. S. Pearson, *Rubber Chem. Technol.*, **60,** 439 (1987).
13. N. R. Langley and K. E. Polmanteer, *J. Pol. Sci. Polym. Phys. Ed.*, **12,** 1023 (1974).
14. M. Inokuti, *J. Chem. Phys.*, **38,** 2999 (1963).
15. D. S. Pearson and W. W. Graessley, *Macromolecules,* **11,** 528 (1978).
16. M. Mooney, *J. Appl. Phys.*, **11,** 582 (1940).
17. A. Havranek and G. Heinrich, *Acta Polym.*, **39,** 563 (1988).
18. J. E. Mark, *Physical Properties of Polymers,* American Chemical Society, Washington, DC, 1984.
19. R. Stadler, V. Abetz, and M. M. Jacobi, *Polym. Bull.*, **14,** 317 (1985).
20. B. M. E. van der Hoff, *Ind. Eng. Chem. Prod. Res. Dev.*, **2,** 273 (1963).
21. M. Cesari, G. Perego, A. Zazzetta, and L. Gargani, *Makromol. Chin.*, **181,** 1143 (1980).
22. R. S. Rivlin, *J. Appl. Phys.*, **18,** 444 (1948).
23. B. Erman and P. J. Flory, *J. Chem. Phys.*, **68,** 5363 (1978).
24. P. J. Flory and B. Erman, *Macromolecules,* **15,** 800 (1982).
25. B. Erman and P. J. Flory, *Macromolecules,* **15,** 806 (1982).
26. J. D. Ferry, *Viscoelastic Properties of Polymers,* 3rd ed., Wiley, New York, 1980.
27. P. J. Flory, *J. Chem. Phys.*, **66,** 5720 (1977).
28. M. L. Williams, R. F. Landel, and J. D. Ferry, *J. Am. Chem. Soc.*, **77,** 3701 (1955).

Received April 21, 1992
Accepted May 27, 1992